JOURNAL OF AIRCRAFT
Vol. 40, No. 4, July–August 2003

Off-Surface Aerodynamic Measurements of a Wing in Ground Effect

Xin Zhang* and Jonathan Zerihan†
University of Southampton, Southampton, England SO17 1BJ, United Kingdom

The off-surface aerodynamic characteristics of a wing in ground effect are investigated using a number of methods including laser Doppler anemometry and particle image velocimetry. The study focuses on two aspects of the flow: turbulent wake and edge vortex. These features are closely associated with the behavior of the aerodynamic force in ground effect. The size of the wake increases in proximity to the ground. A downward shift of the path of the wake is also observed. Discrete vortex shedding is seen to occur behind the wing. As the wing height is reduced, separation occurred on the suction surface of the wing, and the spanwise vortex shedding is found to couple with a flapping motion of the wake in the transverse direction. An edge vortex is also observed off the edge of the end plate of the wing, which contributes to force enhancement and helps to define the force behavior in the force enhancement region. The rate of change in the downforce vs height curve is linked to the strength of the edge vortex. The vortex breakdown signals a slowdown in the force enhancement. When the maximum downforce height is reached, the edge vortex breaks down completely.

Nomenclature

b	=	wing span
C_L	=	overall downforce coefficient, $L/q_\infty S$
C_{Lcent}	=	section downforce coefficient at wing center
C_{Ltip}	=	section downforce coefficient at wing tip
C_P	=	pressure coefficient, p/q_∞
c	=	wing chord
d_v	=	size of vortex
h	=	model height
$h_{\text{max force}}$	=	model height at maximum downforce
$h_{\text{max rate}}$	=	model height at which the maximum rate of downforce enhancement occurs
L	=	downforce (lift)
p	=	pressure
q_∞	=	dynamic head, $\rho_\infty U_\infty^2/2$
Re	=	Reynolds number, $\rho U_\infty c/\mu$
S	=	platform area
U_∞	=	freestream velocity
u, v, w	=	velocity components in x, y, z axes system
u_m	=	minimum in wake velocity profile
uu	=	turbulent normal stress
uv	=	primary shear stress
x, y, z	=	Cartesian coordinates, x +ve downstream, y +ve up, z +ve to starboard
Δ	=	wake thickness
Δ_b	=	lower limit of the wake
Δ_t	=	upper limit of the wake
η	=	normal distance to the wall
μ	=	viscosity
Ω_x	=	streamwise vorticity, $(\partial w/\partial y - \partial v/\partial z)c/U_\infty$
Ω_z	=	spanwise vorticity, $(\partial u/\partial y - \partial v/\partial x)c/U_\infty$
ρ	=	density

Received 6 February 2002; revision received 24 February 2003; accepted for publication 5 March 2003.

*Professor of Aerodynamics, Aeronautics and Astronautics, School of Engineering Sciences. Senior Member AIAA.

†Research Student, Aeronautics and Astronautics, School of Engineering Sciences; currently Aerodynamicist, B.A.R., Brackley, Northants, NN17 7BD, U.K.

Introduction

A CAMBERED wing with its suction surface nearest to a flat surface possesses aerodynamic features of both practical and fundamental interest. It can be found on a racing car operating in ground effect to increase downforce. The downforce works in conjunction with the mechanical grip to improve the acceleration, braking, and cornering speed of the car. In terms of aerodynamic performance, there are three main issues deserving attention: 1) the downforce in ground effect, 2) the turbulent wake generated off the trailing edge of the wing, and 3) the edge vortex generated off the edge or tip of the wing. In terms of 1), both the absolute level and the rate of change in ground effect are important.[1] The downforce is in turn affected by 2) and 3). Moreover, the turbulent wake and edge vortex influence, to a large extent, the aerodynamic performance of the wheels, undertray, side-pods, radiators, diffuser, and rear-wing assembly, as they all operate in the wake and vortices from the front wing.

It is therefore important to study the off-surface aerodynamic performance of a wing in ground effect. However, there is a lack of public domain data on wings in ground effect that are supposed to simulate correctly the flow around a racing car front wing. Because of the severe effect of the ground, fixed ground tests are not believed to be of significantly more use than tests in freestream. Without a good understanding of the major physics, computational modeling effects are deemed to be of little value. Knowles et al.[2] performed an experimental study of a single-element wing with the suction surface near to a moving ground. However, no three-dimensional effects or off-surface flowfield data were presented. Recently, Zerihan and Zhang[1,3] conducted the first systematic study of a wing in ground effect, including both single- and double-element wings. The current study is a part of a series of studies into the wing-in-ground effect. It follows an earlier study on the two-dimensional aerodynamic features of the wing-in-ground effect. The focus of the study is the turbulent wake and edge vortex from the wing.

In terms of the turbulent wake, the existence of vortex shedding on wings with a finite trailing-edge thickness has been well publicized.[4–6] Pailhas et al.[4] have investigated a thick trailing-edge aerofoil using laser Doppler anemometry (LDA), and found the mean flowfield to be characterized by two counter-rotating vortices downstream of the trailing edge. Koss et al.[7] obtained similar results. The authors compared the flowfield to the mean flow behind a Gurney flap, a twin vortex pair. High levels of normal stress uu were found, in two distinct peaks, in the near-field wake region. Jeffrey et al.[8] showed that the flowfield behind a Gurney flap was characterized by a wake of alternately shedding vortices. A recent work

by Zhang and Zerihan[9] illustrated the vortex structure downstream of a Gurney flap fitted to a wing in ground effect.

In this study both LDA and particle image velocimetry (PIV) were employed to perform a detailed off-surface survey of the wake and edge vortex. Results are used 1) to establish a link between the force on the wing and off-surface aerodynamic features and 2) to assess the likely effect of the wake and the edge vortex on trailing aerodynamic components.

Description of Experiments

Wind Tunnel

Experiments were performed in the University of Southampton 3.5 m $\times$ 2.5 m R. J. Mitchell tunnel for the LDA surveys and 2.1 $\times$ 1.7 m wind tunnel for the other results. Both of the tunnels are of a conventional closed-jet, closed-circuit design. For correct modeling of the ground plane, the tunnels are equipped with a large, moving belt rig. A system is located upstream of the belt for removal of the boundary layer that grows along the floor of the wind tunnel. The boundary layer is sucked away through a slot and a perforated plate. With the boundary-layer suction applied, the velocity reaches the freestream value less than 2 mm from the ground, corresponding to $h/c < 0{\cdot}01$. The freestream turbulence level in the wind tunnels is less than 0.2%.

Wing Model

The tests were performed on a single-element, untapered, untwisted rectangular wing of span 1100 mm and chord 223.4 mm, corresponding to an aspect ratio of approximately five. End plates were used throughout testing (see Fig. 1 and Ref. 1). The wing profile was the main element of the Tyrrell 026 Formula 1 car front wing. The current wing profile has evolved over a large period in time, from a GA(W)-type wing.

The model was designed as an 80%-scale model. The test speed of 30 m/s and model size correspond to Reynolds numbers in a range approximately 20–50% higher than current racing car testing. The actual Reynolds number tested, based on the chord of the wing, falls into a range of 0.430–0.462 $\times$ 10^6 because of fluctuations in ambient conditions. The tests were performed at constant velocity.

All LDA and PIV tests were performed on a clean wing, without pressure taps. Transition fixing was performed using strips of #100 grit 1.3%c wide at 10%c from the leading edge on both surfaces. In addition to the standard experimental reasons for fixing transition, the relatively low test Reynolds-number results in a separation bubble over about 5% of the aerofoil chord for the free transition case, which would cause problems for computational-fluid-dynamics modeling purposes. The results are also of fundamental interest, as it is common for the wing to pick up dirt, dust, and debris throughout the race.

Experimental Procedures and Systems

Results for LDA and PIV tests presented here were performed for a range of heights in the force-enhancement and force-reduction regions, from $h/c = 0{\cdot}067$ to 0·448. The height is defined as the distance from the ground to the lowest point on the wing, with the wing incidence set to 0 deg. The incidence of the wing is varied using a rotation about the quarter-chord position. The reference incidence of 3.45 deg is the incidence corresponding to end plates parallel to the ground, with the wing in its datum position.

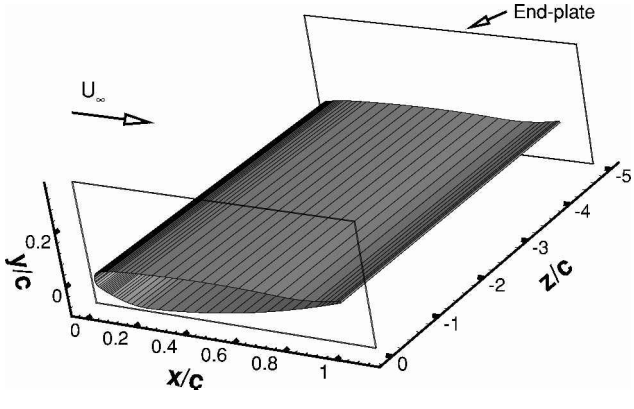

Fig. 1 Schematic of the wing with end plates.

Near-field LDA surveys were performed over an area from above the trailing edge to the ground plane, in the vertical direction, extending from the trailing edge to $x/c = 1{\cdot}2$ in the chordwise direction, with approximately 500 points in the grid. A fine grid spacing is used near to the trailing edge and the ground. Far-field wake surveys were performed at three chordwise positions, corresponding to $x/c = 1.5$, 2.0, and 3.0. The space between points is reduced both in the region of the wing's turbulent wake and is further reduced very close to the ground. Approximately 70 points are used in each wake survey. In addition to this, a selection of boundary-layer surveys was performed on the suction surface at the trailing edge.

The LDA measurements are performed with a three-component Dantec system with a 5-W Ar-ion laser. The system is operated in backscatter mode. The velocities measured in the beam axes are resolved into the tunnel coordinate system (x, y, z) using a matrix transformation. Seeding is introduced by three seeding generators located downstream of the rolling road, behind the model. The LDA signals are analyzed using three Dantec Burst Spectrum Analysers. Generally, more than 800 bursts (instantaneous samples) are collected for each data point.

To investigate unsteady flow features, PIV measurements were performed using a Dantec PowerFlow system. The region of the flowfield including the trailing-edge region, from the ground to above the wing, that extends to $x/c = 1{\cdot}8$ at the wing semispan is mapped. To facilitate optical access, a Perspex endplate is used. To illustrate the flowfield phenomena of interest, results had to be processed on a very fine grid with a spacing between grid points that corresponds to 1.48 mm (0.0066c). This leads to some noise in the results, especially where measurements are taken through the endplate. The analysis sequence used was to first cross-correlate the data on 32 $\times$ 32 pixels and then to perform a range validation of the resulting vectors on a 157 $\times$ 125 grid. No filtering was used as this was found to "blur" the results significantly in regions of high velocity gradients.

Errors and Uncertainties

The incidence of the wing is set to within $\pm 0{\cdot}005$ deg, and the height is set to within $\pm 0{\cdot}2$ mm. Belt-lifting was not observed under the flow conditions tested. The tunnel is run at a constant dynamic pressure of 56.25-mm water $\pm 0{\cdot}05$. Using procedures detailed by Moffat,[10] the errors in C_L were calculated using the addition method within a 95% confidence; the worst case occurs at a height of 0.056c and corresponds to a C_L of $1{\cdot}678 \pm 0{\cdot}009$.

Estimations of the 95% confidence interval in the LDA results were conducted using procedures given by Benedict and Gould.[11] Typical values in the turbulent wake are $\pm 0{\cdot}0004$ for the turbulence stresses uu/U_∞^2 and uv/U_∞^2. Further away from the center of the wake, the uncertainty typically decreases as the levels of turbulence reduce. The smoothness of the results suggests that the actual errors are significantly less than the quoted values for the uncertainty. A comparison of LDA and PIV measurements is made in terms of wake profile. The maximum velocity deficits in the wake are very similar, and outside the boundary layer the velocities also agree well.

Results and Discussions

Both free-transition and fixed-transition (at 10% chord) cases were extensively studied. However, fixed-transition results are mainly presented as they are a better case for numerical model validation. The major physical features, though, remain the same for both cases. Where possible, the free-transition data are used to support the interpretation of the results, and their use is clearly stated in the text. The wake measurements are made in the symmetrical plane of the wing.

Review of Force Behavior

In a recent study the behavior of the aerodynamic force and pressure of a single-element wing in ground effect has been discussed.[1] Hence, we will not repeat the findings in details. The effect of the ground is to constrain the flow beneath the suction surface. At a large height in ground effect, the flow is therefore accelerated more over the suction surface than for the wing out of ground effect in freestream. This results in greater suction on the suction surface. As the wing is brought closer to the ground, the flow is even more accelerated, which causes an increased peak suction and a higher pressure recovery demand. At a critical height where the pressure recovery is sufficiently steep, boundary-layer separation occurs at the trailing edge of the suction surface. For the free-transition case this occurs at $h/c = 0.224$. As the height is reduced below this height, the wing still generates more downforce, and the downforce will reach a maximum, as a result of large-scale separation, that is, stall. Below $h_{\max\ force}$ the downforce reduces, which is commonly referred to as the the downforce reduction phenomenon. As the height is reduced from the first height at which flow separation is observed, the separation point moves forward steadily. At the maximum downforce the boundary layer separates at approximately 80%c for the free-transition case. Heights greater than $h_{\max\ force}$ are known as the force-enhancement region. Heights below $h_{\max\ force}$ are in the force-reduction region. An analogy can be drawn between the reduction of the height of a wing above the ground and the increase of the incidence of a wing in freestream. In both cases the pressure recovery becomes steeper, eventually causing boundary-layer separation and the wing to stall. The effect of fixing transition is to reduce the magnitude of the downforce and to increase the height at which the force-reduction phenomenon occurs.

Off-Surface Wake Measurements; Unsteady Flow

Figure 2 shows instantaneous vorticity contours at model heights of $h/c = 0.448$, 0.179, 0.134, and 0.067. The results represent a typical snapshot of the unsteady flowfield.

At $h/c = 0.448$ the wake formed by the flow separation from both the pressure and the suction surfaces is characterized by concentrated areas of high and low vorticity, which indicate the presence of discrete vortices. At a height of $h/c = 0.179$, the discrete vortex shedding is again observed, although the structure of the vortex shedding is different from that at $h/c = 0.448$. The discrete vortices emanating from both the pressure and suction surfaces are larger and stronger than for the case at the greater height. However, they appear less ordered. The separation between consecutive vortices is increased. At a height of $h/c = 0.134$, all of the vortices appear stronger, less regular, and more chaotic. The formation of the first vortex seems to be delayed, and for a short distance the wake appears similar to an unstable shear layer with a flapping motion in the transverse direction. At $h/c = 0.067$ the change is amplified again, and the unstable shear layer lasts to $x/c = 1.2$.

The vorticity contours at the different heights are similar to the observation of the flow behind a Gurney flap on a wing in ground effect (see Zhang and Zerihan[9]). As the boundary layer on the suction surface thickens, as a result of increasing ground proximity, the vortices become larger. The alternate vortex shedding is found to break down in close proximity to the ground and is accompanied by the separation of the suction surface boundary layer. The wake experiences a transverse flapping motion, which grows in extent downstream.

The current results highlight the existence of vortex shedding behind a wing with a finite trailing edge. It is difficult to estimate the discrete frequency of the vortex shedding. Results behind the Gurney flap do yield a discrete frequency for the shedding.[9] Of significance regarding vortex shedding is the thickness of the separating shear layers with respect to the distance between the shear layers. From LDA results the time-averaged value of the boundary-layer thickness at the trailing edge of the suction surface is found to be approximately 0.05c for a typical height in the force-enhancement region. The thickness of the finite trailing edge is 0.007c. The height of the Gurney flap gives a distance of 0.029c between the shear layers at the trailing edge. The thickness of the boundary layer at the trailing edge (of the suction surface) varies with time because of its unsteady nature. The range of the ratios of the boundary-layer thickness to the distance between the shear layers is larger for the clean wing than for the wing with the Gurney flap. This implies that the vortex shedding for the clean wing with the finite trailing edge will be less regular than for the wing with the Gurney flap, in terms of the discrete frequency at which the vortices are shed. Indeed, Vassilopoulos and Gai[5] found that a turbulent boundary layer which increased the shear-layer instability had the effect of increasing the number of discrete shedding frequencies.

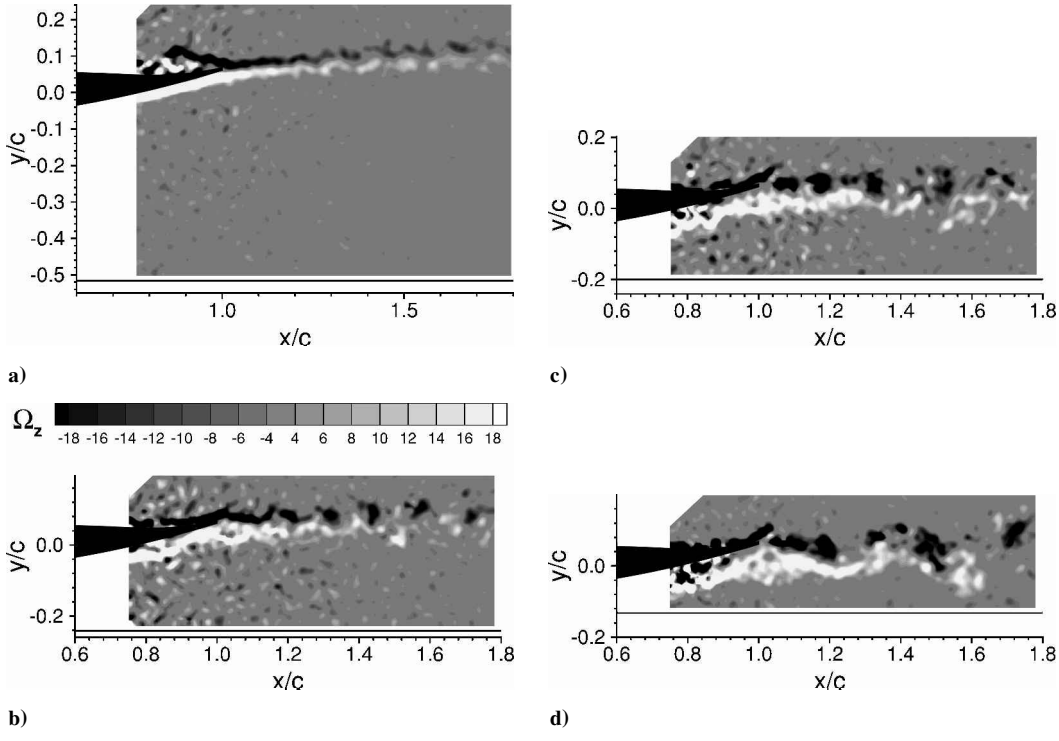

Fig. 2 Instantaneous spanwise vorticity Ω_z contours. Free transition: a) $h/c = 0.448$, b) $h/d = 0.179$, c) $h/d = 0.134$, and d) $h/d = 0.067$.

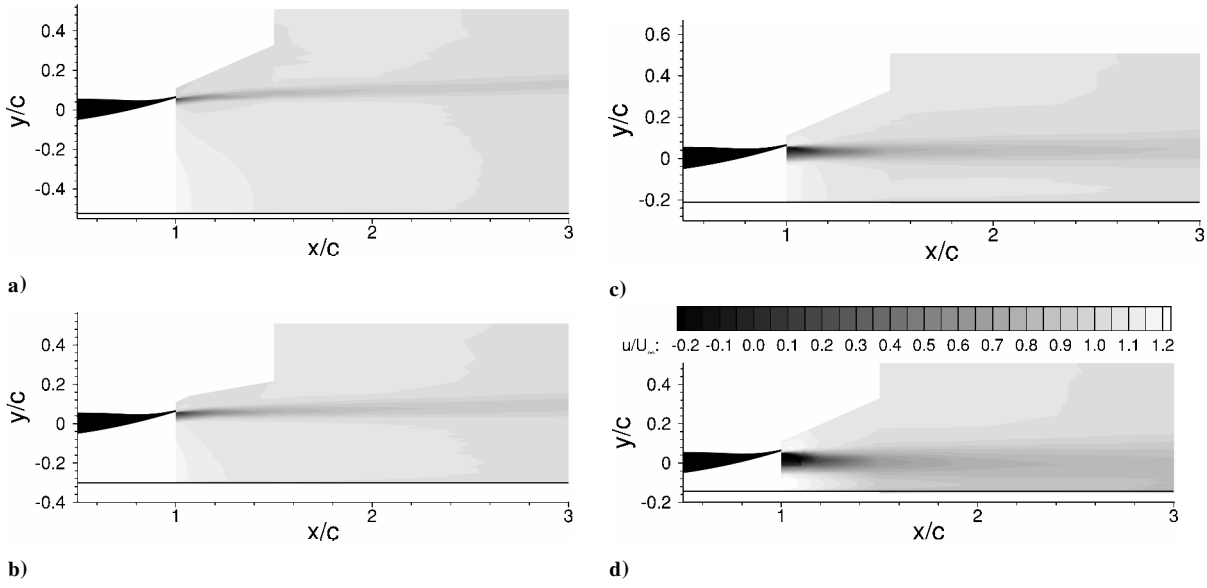

Fig. 3 Mean streamwise velocity u/U_∞ contours. Free transition: a) $h/c = 0.448$, b) $h/d = 0.224$, c) $h/d = 0.134$, and d) $h/d = 0.067$.

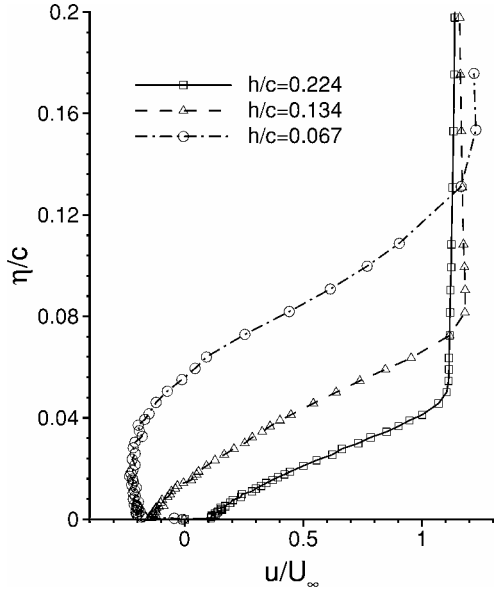

Fig. 4 Time-averaged boundary-layer profiles, taken at trailing edge on suction surface. Fixed transition.

Table 1 Wake characteristics

h/c	x/c	u_m/U_∞	y at u_m	y at Δ_t	y at Δ_b	Δ
0.448	1.5	0.81	0.08	0.13	0.04	0.09
	2.0	0.90	0.10	0.16	0.04	0.12
	3.0	0.93	0.13	0.22	0.06	0.16
0.313	1.5	0.81	0.08	0.13	0.04	0.09
	2.0	0.89	0.09	0.16	0.04	0.13
	3.0	0.93	0.14	0.22	0.04	0.18
0.224	1.5	0.79	0.07	0.13	0.01	0.11
	2.0	0.88	0.08	0.16	0.01	0.15
	3.0	0.93	0.12	0.20	0.01	0.19
0.179	1.5	0.78	0.05	0.12	−0.02	0.14
	2.0	0.88	0.06	0.15	−0.03	0.18
	3.0	0.91	0.07	0.19	−0.03	0.22
0.134	1.5	0.77	0.04	0.12	−0.05	0.17
	2.0	0.85	0.04	0.14	−0.07	0.21
	3.0	0.91	0.05	0.19	−0.08	0.27
0.112	1.5	0.73	0.04	0.13	−0.07	0.20
	2.0	0.85	0.04	0.16	−0.08	0.24
	3.0	0.91	0.06	0.20	−0.10	0.30
0.090	1.5	0.72	0.02	0.12	−0.10	0.22
	2.0	0.84	0.02	0.16	−0.11	0.27
	3.0	0.90	0.01	0.19	−0.12	0.31
0.067	1.5	0.66	0.00	0.13	−0.11	0.23
	2.0	0.77	−0.01	0.17	−0.10	0.27

Time-Averaged Off-Surface Flow

Figure 3 presents time-averaged LDA results for the u/U_∞ velocity contours for the wing in ground effect at four heights in both force-enhancement and force-reduction ranges. The general flow features of interest can be seen qualitatively. The wake becomes thicker as it moves downstream, with the velocity deficit reducing as a result of turbulent mixing. As the ground is approached, the wake increases in size, and the velocity deficits become larger. In addition to this, the path of the wake changes, such that its angle of incidence reduces with increasing ground proximity. Between the wake and the ground, the flow encounters an adverse pressure gradient, which is especially visible in the region $x/c = 1.0 - 1.5$. For the smallest height shown in Fig. 3, $h/c = 0.067$, the wake from the wing merges with the ground plane at $x/c = 1.5$. This height is below $h_{\max\ \text{force}}$.

Boundary-layer profiles taken on the suction surface at the trailing edge of the wing (Fig. 4) show the thickening of the boundary layer as the height is reduced; this thickening results from the increase in peak suction and the associated adverse pressure gradient. For the $h/c = 0.224$ case the boundary layer is very close to separation. The results at the two lower heights clearly show separation.

Figure 5 shows a series of wake surveys performed at various heights. For clarity, the symbols represent only every other data point. At heights of $h/c = 0.448$ and 0.224, two typical heights in the force-enhancement region, the size of the wake increases as it evolves downstream. At $h/c = 0.224$ the velocity at the maximum velocity deficit increases from $u/U_\infty = 0.79$ at $x/c = 1.5$ to 0.88 at $x/c = 2.0$ and 0.93 at $x/c = 3.0$. The height at which this occurs increases from $y/c = 0.06$ to 0.08 and 0.11 for the three locations, as the height of the wake increases, as can be seen in the streamwise velocity contours (Fig. 3). The height at the top of the wake is defined as the location where the velocity is 99% of the velocity outside the wake; this height increases from $y/c = 0.13$ to 0.16 and 0.20 at the three locations. In comparison, the height at the bottom of the wake remains approximately constant at $y/c = 0.01$. The thickness of the wake increases from $\Delta = 0.11$ to 0.15 and 0.19. Information regarding the growth of the wake for several different heights is tabulated in Table 1. For the lower heights at $h/c = 0.134$ and 0.067, the position of the maximum velocity deficit no longer rises as much

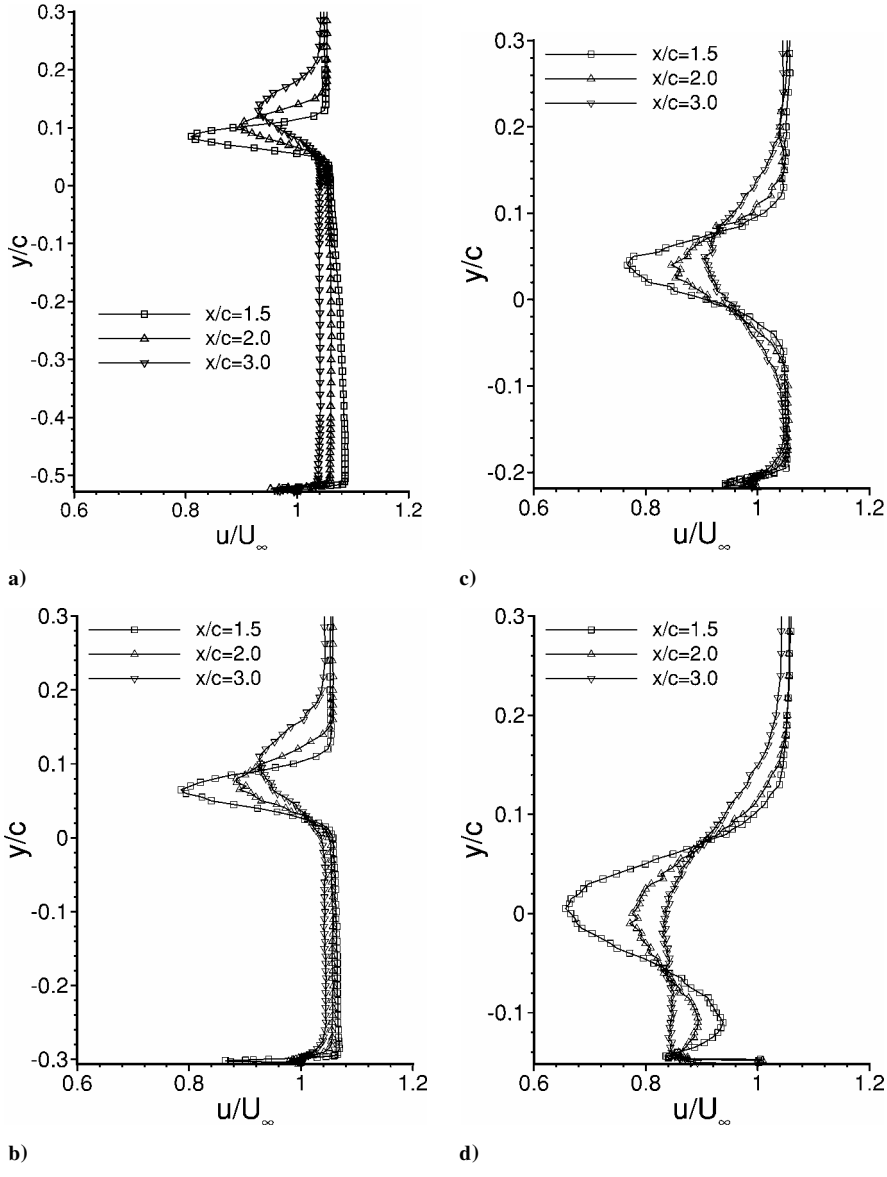

Fig. 5 Mean flow u/U_∞ velocity wake profiles: a) $h/c = 0.448$, b) $h/d = 0.224$, c) $h/d = 0.134$, and d) $h/d = 0.067$.

as the wake evolves downstream. In Fig. 5a, the growth of the ground boundary layer can now be detected, though it remains very small. As the height is reduced, the growth of the ground boundary layer is clear. The wake and the ground boundary are merged at $h/c = 0{\cdot}067$, a height in the force-reduction region.

For a height of $h/c = 0{\cdot}448$, the normal turbulent stress uu and primary shear stress uv are presented in Fig. 6. The normal stress distribution is characterized by a twin peak profile, as a result of separated shear layers from the suction and pressure surfaces. As the wake evolves downstream, the magnitudes of the peaks decrease, although at $x/c = 3{\cdot}0$ the basic shape of the distribution is retained. The primary shear-stress distribution shows two peaks of opposite signs. The strong turbulent mixing level in the wake ensures the spread of the wake. The upward movement of the wake caused by the pressure difference across the wake is also observed.

The effect of changing the height of the wing above the ground on the wake at $x/c = 1{\cdot}5$ is shown in Fig. 7. The wake grows significantly as the ground is approached from $\Delta = 0{\cdot}09$ at $h/c = 0{\cdot}448$ to 0.11 at $h/c = 0{\cdot}224$, 0.17 at $h/c = 0{\cdot}134$, and 0.23 at $h/c = 0{\cdot}067$. Again, these data are summarised in Table 1. For the smallest height $h/c = 0{\cdot}067$, the wake has merged with the ground boundary layer, and the quoted size for the thickness is not strictly valid. For the next height $h/c = 0{\cdot}090$ (not illustrated here); the wake appears close to merging with the ground. The location of the top of the wake remains constant at $y/c = 0{\cdot}12$. However, the bottom reduces height from $y/c = 0{\cdot}04$ for the greatest ride height to $-0{\cdot}11$ for the smallest height. This has the effect of lowering the height at which the maximum velocity deficit occurs as the ground is approached. The maximum velocity deficit also increases.

As the model height is reduced, the adverse pressure gradient increases, eventually leading to separation, as just shown. Hence, as the height is reduced, the boundary layer on the suction surface is increased, and hence the wake increases in size. It is this mechanism that causes the wake to grow as the ground is approached, because of the observed change in only the location of the bottom of the wake.

Very close to the ground, a deficit in velocity is seen in Fig. 7. This forms part of the ground boundary layer, extending towards the values of constant velocity. The fact that the ground moves with velocity $u/U_\infty = 1{\cdot}0$ implies that the region of velocity deficit is actually a separated flow region on the ground. For the practical case the flow separating on the ground will tend to pick up dust and disperse it into the surrounding flow. Because of the very fine spacing between measurement points and steep velocity gradients, it is difficult to compare the velocity deficit part of the ground flow in terms of velocity. However, the thickness of the separated flow region can be seen to increase with close proximity to the ground. It is believed that this is formed as a result of flow very close to

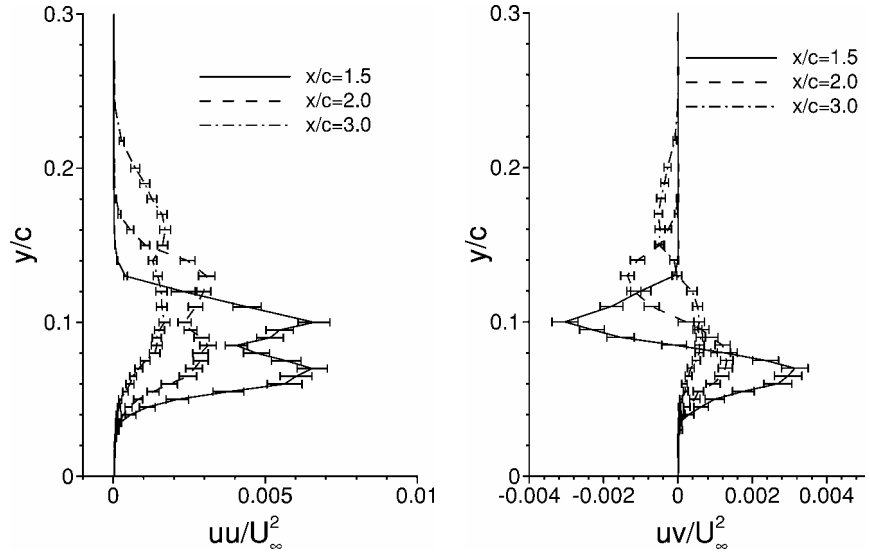

Fig. 6 Wake development at $h/c = 0.448$: a) normal turbulent stress uu and b) primary shear-stress uv.

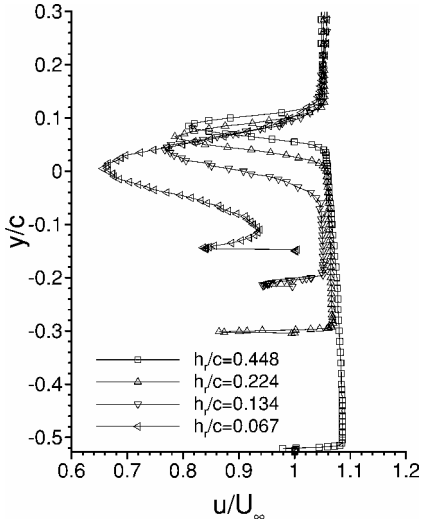

Fig. 7 Wake profiles at various model heights: $x/c = 1.5$.

the ground retarding, caused by the adverse pressure gradient encountered from the point of maximum suction. As just stated, the adverse pressure gradient increases with ground proximity, which enforces this hypothesis. In fact, the flow exhibits features similar to a wall-jet-type flow.

Figure 8 shows profiles of the normal stress uu and primary shear stress uv from the wake surveys at $x/c = 1{\cdot}5$. As expected, the turbulent wake features high levels of uu. As the wake becomes larger, because of the smaller height, the stresses become larger. Two peaks are at each height. For the three larger heights the two peaks are approximately the same in magnitude. However, for the smallest height $h/c = 0{\cdot}067$ the lower peak seems significantly larger than the upper peak. These are attributed to the vortex shedding. At the smallest height of $h/c = 0{\cdot}067$, the increased size of the lower peak arises from the separated suction surface boundary layer. Similar pairs of peaks in the uu distribution were found in work by Koss et al.,[7] using LDA in the near-wake region of a divergent trailing-edge aerofoil. As the ground is approached, the magnitude of the fluctuating velocity increases for all cases except the height closest to the ground. Although not illustrated here, results at $h/c = 0{\cdot}090$ show a higher peak uu value than that at $h/c = 0{\cdot}067$. The results taken close to the ground in the region between the ground plane and the constant velocity accelerated fluid region suggest that the ground flow region, including the velocity deficit area, is turbulent in nature.

Further Discussion of Wake Survey

Aerodynamic interactions between the wake from the front wing and the downstream devices are critical to the performance of the overall vehicle. For example, the wake from the front wing can be ingested into the side-pods and severely affect the efficiency of the radiators used for cooling of the mechanical devices. The flow to the undertray that leads to the diffuser and the rear wing is also significantly affected by the front wing wake.

The results show that, at a large height from the ground, a small wake results with relatively low levels of turbulence results. This is desirable from the point of view of the downstream devices. The downforce generated at this height from the ground, unfortunately, is significantly lower than that which could be generated in closer proximity to the ground. However, the large wake that occurs at small model heights results in higher levels of turbulence and more mixing in the wake. This higher freestream turbulence significantly affects the performance of the downstream aerodynamic devices. Moreover, the presence of the flapping motion in the shear layer from the suction surface points to the meandering of the large, discrete vortices. The wake survey shows the generation of a ground boundary layer as the wing is lowered to the ground, as a result of adverse pressure gradient. As large vortices travel downstream, they are likely to interact with the ground boundary layer, resulting in a highly unsteady flowfield. The performance of trailing aerodynamic components could thus be adversely affected.

Edge Vortex

The existence of a main edge vortex is illustrated in Fig. 9 in which the results of a LDA survey behind the wing are given.[12] In the figure both the streamwise velocity (contours) and the crossflow velocity (vectors) are presented. The extent of the survey covers an area extending from the center of the wingspan to the end plate. The results show the turbulent wake region behind the wing. Towards the center of the wingspan, a two-dimensional flowfield can be established. The edge vortex dominates the flow in the vicinity of the end plate. An important feature is the low streamwise speed core of the edge vortex, as the vortex is formed by the separation of the flow on the end plate. This feature is important as the vortex could breakdown or dissipate quickly further downstream.

Earlier, the downforce behavior is reviewed. The force measurements presented in Zerihan and Zhang[1] show the effect of height on the force coefficients. The drag coefficient increases with a reduction

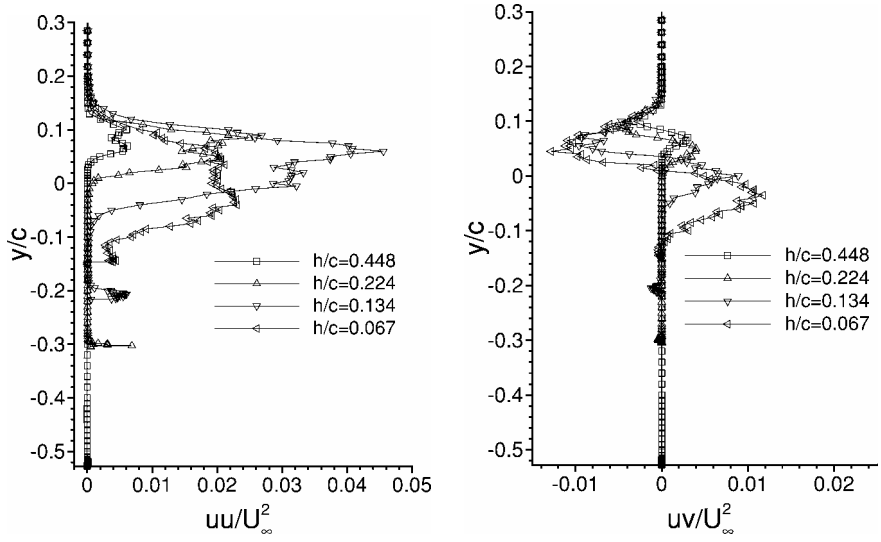

Fig. 8 Wake profiles at various model heights: a) normal turbulent stress *uu* and b) primary shear-stress *uv*.

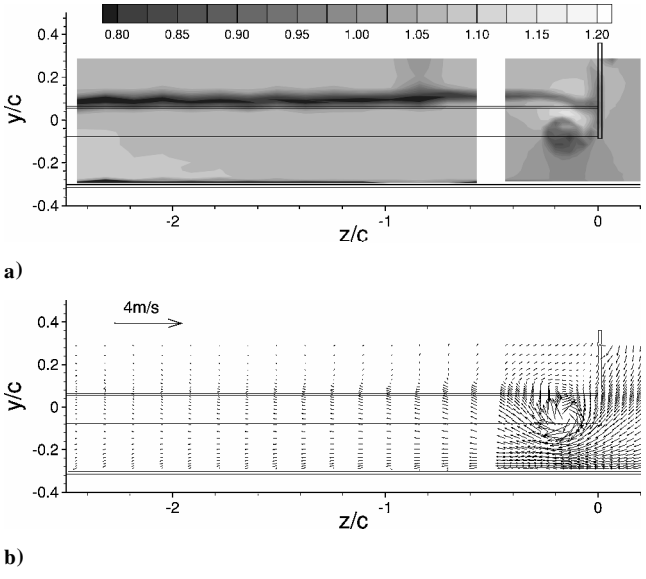

Fig. 9 Cross-plane LDA survey of edge vortex at *x/c* = 1.5. Fixed transition: a) streamwise velocity and b) velocity vectors (Fig. 2, Ref. 12).

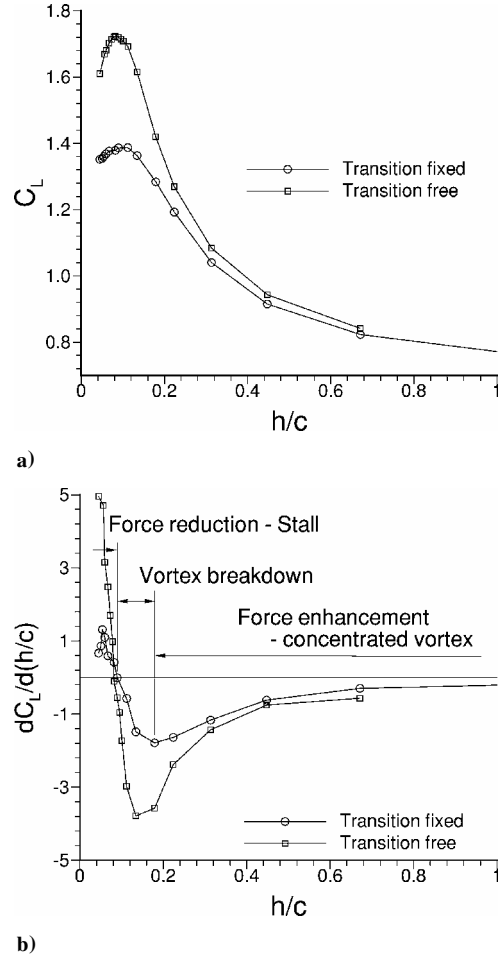

Fig. 10 Force behavior with model height: a) downforce and b) rate of change in downforce.

in the height. The downforce coefficient first experiences an increase, that is, the force-enhancement phenomenon, and then a reduction, that is, the force-reduction phenomenon. The maximum in downforce is reached at $(h/c)_{\text{max force}} = 0{\cdot}082$ for the free-transition case and $(h/c)_{\text{max force}} = 0{\cdot}0895$ for the fixed-transition case. The main cause of the force reduction was found to be the suction surface separation at the lower ride height. What is interesting is the behavior of the downforce near the maximum downforce height, as illustrated by Fig. 3 in Zerihan and Zhang.[1] Although the drag coefficient increases as the wing is moved to the ground, the rate of drag increase rises as the ground is approached; the rate of downforce enhancement actually slows down before the maximum is reached. This phenomenon is illustrated in Fig. 10, where the rate of downforce change with the ride height is shown. It is seen that the downforce enhancement increases rapidly initially until a maximum is reached, well before the height of maximum downforce. For the free-transition case the height is $(h/c)_{\text{max rate}} = 0{\cdot}134$, and for the fixed-transition case, $(h/c)_{\text{max rate}} = 0{\cdot}179$. Between this height and the maximum downforce height, the downforce enhancement still persists but at a slower rate.

It seems that between the $h_{\text{max force}}$ and $h_{\text{max rate}}$ there exists a region that has important considerations for design. On one hand, the mechanism of downforce enhancement can be employed; on the other hand, the rate of downforce change can be controlled to minimize some less desirable effects, such as high pitch sensitivity.

Figure 11 points to the critical region of the flow where $h_{\text{max rate}}$ is determined. The figure shows downforce behavior of a free-transition case. Both the overall and the section force coefficients are included in the figure. For this case suction surface separation first appears at $h/c = 0{\cdot}224$ (Ref. 1). However, the downforce

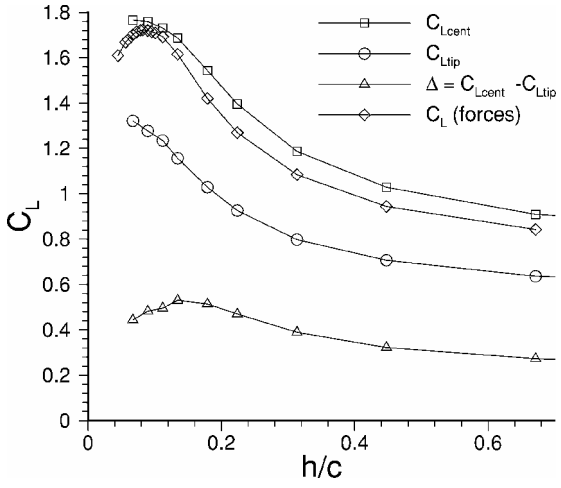

a)

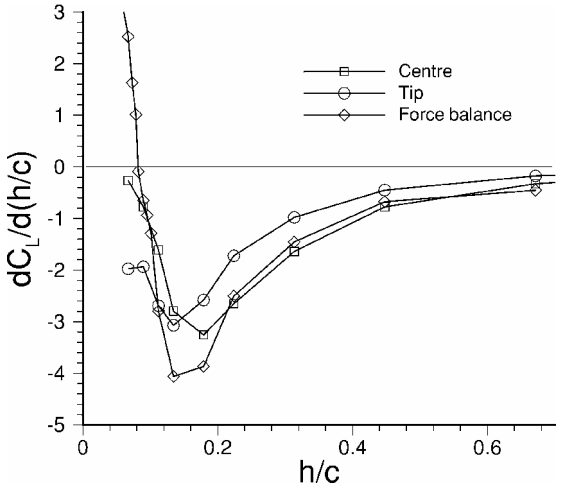

b)

Fig. 11 Downforce behavior of the free-transition wing: a) downforce (Fig. 11, Ref. 1) and b) rate of change in downforce.

enhancement still persists, and the rate of downforce enhancement continues to rise as well. At $h/c = 0.179$ the rate of change in C_{Lcent} reaches its maximum absolute value in the enhancement region. The suction surface separation has now reached a large enough extent to affect the force behaviors near the center of the wing. The rate of change in C_L and C_{Ltip}, though, will not reach their absolute maximum values together until $h/c = 0.134$. It is apparent that flow near the tip of the wing defines $h_{\text{max rate}}$.

In this study, the variation of the downforce enhancement rate is linked in this study to the generation, evolution, and breakdown of edge vortices of the wing. The existence of the edge vortex is illustrated by both surface oil visualization (Fig. 12) and PIV surveys (Figs. 13 and 14). Figure 12 shows an oil flow visualization of surface flow streaklines on the suction surface of the fixed transition wing at $h/c = 0.179$. Towards the midspan of the wing, separation occurs near the trailing edge at this height. The surface streaklines do not feature significant spanwise components near the center span. The flow over the central portion can be regarded as quasi-two-dimensional (not shown in Fig. 12). Significant three-dimensional effects are observed near the tip, which are associated with the presence of the edge vortices. It is conceivable that the pressure field could be affected near the center. However, the presence of the edge vortex has the major effect of delaying the suction surface separation.

In Fig. 13, the edge vortex for the transition fixed wing is shown at two typical heights: one in the force-enhancement region ($h/c = 0.313$) and the second at the maximum downforce height ($h/c = 0.09$). In the force-enhancement region the pressure difference across the side plates leads to flow entrainment between the ground and the end plate. The boundary layer separates at the edge of the plate forming a shear layer. The rolling up of the separated shear layer forms an attached vortex inside the end plate, which then trails downstream. This process is shown in Fig. 13a. The surface flow visualization (Fig. 12) confirms this observation. The flow on the suction surface nearest to the end plate stays attached. There exists an induced, secondary vortex flow at the junction between the suction surface and the end plate. From the surface streaklines it

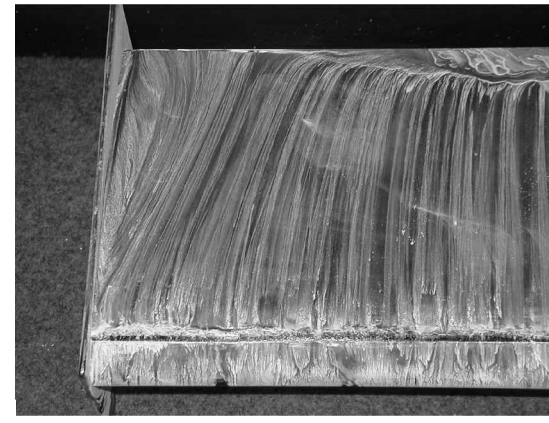

Fig. 12 Surface flow on suction surface at *h/c* = 0.179. Fixed transition. Flow direction upward.

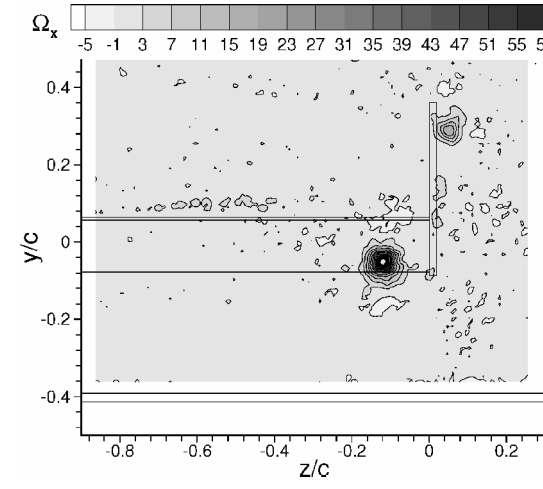

a)

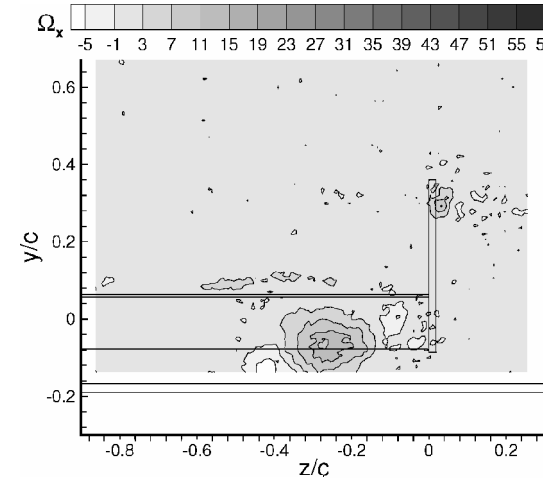

b)

Fig. 13 Edge vortex in ground effect at *x/c* =1.5. Fixed transition: a) *h/c* = 0.313 and b) *h/c* = 0.009.

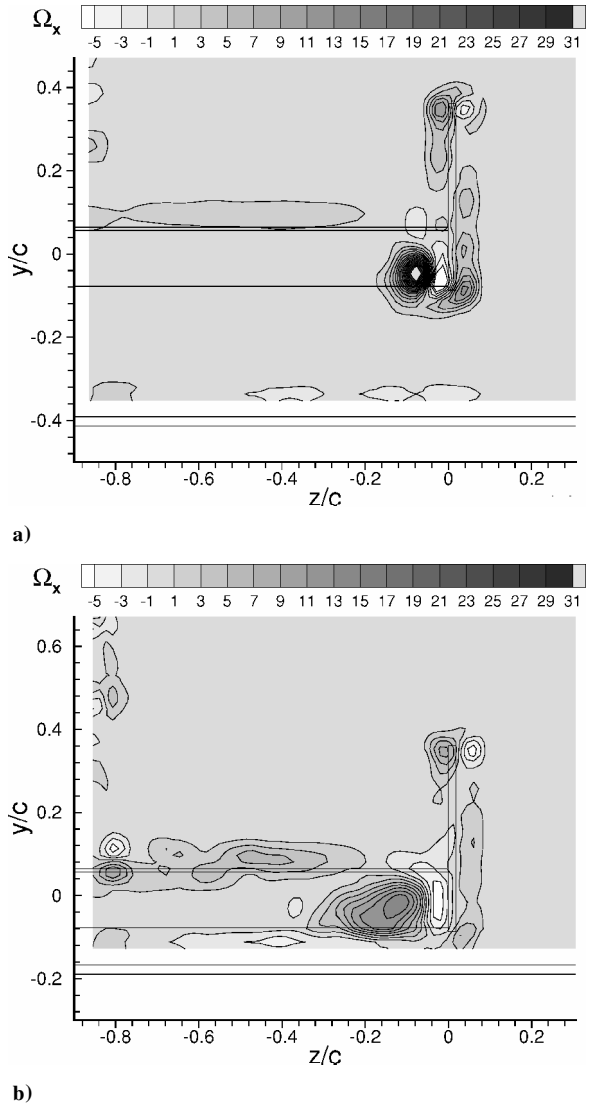

Fig. 14 Edge vortex in ground effect at x/c = 1.2. Free transition: a) h/c = 0.313 and b) h/c = 0.009.

can be seen that the main vortex is initiated from the position of the peak suction on the suction surface, at the junction of the end plate and the suction surface. It then grows along the end plate. There is vortex-induced suction on both the suction surface and the inside of the end plate. The nonlinear component in the downforce is attributed to the vortex-induced suction. Indeed the drag coefficient follows the same trend as the downforce, suggesting an induced drag (vortex drag) contribution.[13] The highly concentrated vortex core points to the presence of a stable vortex flow.

When the model is placed near the maximum downforce height, the vortex moves inboard. Its size increases significantly (Fig. 13b). Indeed, the vortex appears to dilate, which is a feature of vortex breakdown.[14] Table 2 summarizes the vortex dimensions and the maximum vorticity level. The vortex is defined using the criteria of Jeong and Hussain,[15] which is based on the existence of locally spiraling or curved streamlines. An equivalent hydraulic diameter d_v, based on the area occupied by the vortex, is then defined. This value is also given in Table 2. In Table 2 the free-transition data are also provided as a reference. This clarifies that the major physical features are similar for the free-transition and the fixed-transition cases. Figure 14 shows the edge vortex behavior at the two heights in Fig. 13. A similar type of edge vortex is present at each height.

It can be seen that the size of the vortex remains relatively unchanged, above the height for the maximum force-enhancement rate. For the fixed-transition wing this occurs at $h/c = 0.179$. For the free-transition wing the height is $h/c = 0.134$. With the force

Table 2 Edge vortex behaviour: vortex size and maximum streamwise vorticity level

	Fixed transition ($x/c = 1.5$)		Free transition ($x/c = 1.2$)	
h/c	d_v/c	$\Omega_{x\|\max}$	d_v/c	$\Omega_{x\|\max}$
0.067	Vortex breakdown	11.0	Vortex breakdown	7.0
0.090	0.172	14.3	0.132	14.9
0.111	——	——	0.128	28.2
0.134	0.071	70.3	0.075	**64.5**
0.179	0.068	**84.1**	0.070	47.6
0.224	0.060	74.8	0.065	45.1
0.313	0.064	73.8	0.057	37.4
0.448	0.067	36.1	0.057	28.9
0.671	0.064	40.5	0.057	22.0
0.716	0.063	43.1	——	——

enhancement there is an increase in the strength of the edge vortex as measured in terms of the vorticity level. The maximum vorticity levels for both the fixed-transition and free-transition cases are reached at $h_{\max\,\text{rate}}$. Vortex meandering and breakdown appear after $h_{\max\,\text{rate}}$, with a substantial rise in the size of the vortex. The vortex breaks down completely at the maximum downforce height.

Conclusions

The instantaneous and time-averaged flow properties of the wake region of a wing in ground effect with a finite trailing edge have been identified. It is seen that at a large model height vortex shedding is identified from instantaneous particle-image-velocimetry flow images. The mean flow shows a small turbulent wake that grows and moves upwards as it travels downstream. As the model height is reduced, boundary-layer separation occurs on the suction surface. The instability of the shear layer produces discrete vortices. The shear layer experiences a coupled motion of flapping in the transverse direction and vortex convection in the streamwise direction. The size of the turbulent wake grows, especially on the suction side, as a result of the boundary-layer separation on the suction surface. This has a turning effect on the wake, such that as the wake develops it comes closer to the ground.

The generation, evolution, and breakdown of wing edge vortex is studied. The presence of the edge vortex plays a secondary role in the downforce enhancement process. However, it contributes to the downforce enhancement and helps to define the force behavior in the force-enhancement region, in particular near the maximum force height. The rate of change in the downforce curve is linked to the strength of the vortex. When the maximum downforce height is reached, the edge vortex breaks down completely.

Acknowledgments

J. Zerihan wishes to thank the Engineering and Physical Sciences Research Council (EPSRC) for providing a studentship. The authors would like to thank Willem Toet of B.A.R. for his support. Technical assistance was given by the Tyrrell Racing Organisation and B.A.R. The efforts of Geoff Thomas in construction of the model are greatly appreciated. The laser Doppler-anemometry data presented in Fig. 9 and fixed-transition data were collected by M. Deviese in his project study.

References

[1]Zerihan, J., and Zhang, X., "Aerodynamics of a Single-Element Wing-in-Ground Effect," *Journal of Aircraft*, Vol. 37, No. 6, 2000, pp. 1058–1064.

[2]Knowles, K., Donahue, D., and Finnis, M., "A Study of Wings in Ground Effect," *Loughborough Univ. Conference on Vehicle Aerodynamics*, Royal Aeronautical Society, London, UK, July 1994, pp. 22.1–22.13.

[3]Zhang, X., and Zerihan, J., "Aerdynamics of a Double Element Wing in Ground Effect," 40th AIAA Aerospace Sciences Meeting and Exhibit, AIAA Paper 02-0834, Reno, NV, Jan. 2002.

[4]Pailhas, G., Sauvage, P., Touvet, Y., and Coustols, E., "Flowfield in the Vicinity of a Thick Cambered Trailing Edge," *Proceedings of the 9th International Symposium on Applications of Laser Techniques to Fluid Mechanics*, Lisbon, Portugal, July 1998, pp. 19.3.1–19.3.8.

[5]Vassilopoulos, K., and Gai, S., "Unsteady Pressures on a Blunt Trailing Edge—End Plate and Boundary Layer Effects," 36th AIAA Aerospace Sciences Meeting and Exhibit, AIAA Paper 98-0418, Reno, NV, Jan. 1998.

[6]Khorrami, M., Berkman, M., Choudhari, M., Singer, B., Lokhard, D., and Brentner, K., "Unsteady Flow Computations of a Slat with a Blunt Trailing Edge," AIAA Space Technology Conf. and Exposition, AIAA Paper 99-1805, Albuquerque, NM, Sept. 1999.

[7]Koss, D., Bauminger, S., Shepshelovich, M., Seifert, A., and Wygnanski, I., "Pilot Test of a Low Reynolds Number DTE Airfoil," 31st AIAA Aerospace Sciences Meeting, AIAA Paper 93-0643, Reno, NV, Jan. 1993.

[8]Jeffrey, D., Zhang, X., and Hurst, D., "Aerodynamics of Gurney Flaps on a Single-Element High-Lift Wing," *Journal of Aircraft*, Vol. 37, No. 2, 2000, pp. 295–302.

[9]Zhang, X., and Zerihan, J., "Aerodynamics of Gurney Flaps on a Wing in Ground Effect," *AIAA Journal*, Vol. 39, No. 5, 2001, pp. 772–780.

[10]Moffat, R., "Contributions to the Theory of Single-Sample Uncertainty Analysis," *Journal of Fluids Engineering*, Vol. 104, June 1982, pp. 250–260.

[11]Benedict, L., and Gould, R. D., "Towards Better Uncertainty Estimates for Turbulence Statistics," *Experiments in Fluids*, Vol. 22, No. 2, 1996, pp. 129–136.

[12]Zhang, X., Zerihan, J., Ruhrmann, A., and Deviese, M., "Tip Vortices Generated by a Wing in Ground Effect," *Proceedings of the 11th International Symposium on Applications of Laser Techniques to Fluid Mechanics*, Lisbon, Portugal, July 2002.

[13]Jones, R., *Wing Theory*, 1st ed., Princeton Univ. Press., Princeton, NJ, 1990.

[14]Lambourne, N., and Bryer, D., "The Bursting of Leading-Edge Vortices—Some Observations and Discussion of the Phenomenon," Aeronautical Research Council, R&M No. 3282, London, April 1961.

[15]Jeong, J., and Hussain, F., "On the Identification of a Vortex," *Journal of Fluid Mechanics*, Vol. 285, 1995, pp. 69–94.